Effect of Cloud Vertical Inhomogeneity on the Retrieval of Cirrus Cloud Temperature and Infrared Optical Depth Using the ASTR

J. E. RUSSELL AND J. D. HAIGH

Space and Atmospheric Physics, Blackett Laboratory, Imperial College, London, United Kingdom

(Manuscript received 24 November 1997, in final form 30 September 1998)

ABSTRACT

A method is described for the retrieval of cirrus cloud temperature and optical depth using thermal infrared data from the Along-Track Scanning Radiometer. The method utilizes above-cloud and nearby clear-sky thermal infrared data at a single wavelength and two different viewing angles and assumes that the cirrus cloud is nonscattering, isothermal, and semitransparent. The sensitivity of the method to small uncertainties in the input parameters is calculated. The effect on the retrieval of vertical inhomogeneity is investigated using idealized models of cirrus cloud vertical structure. It is shown that a vertical temperature structure within the cloud, alone and in conjunction with vertical inhomogeneity in absorption coefficient, can cause large errors in the retrieved quantities for a wide range of cloud types. However, these investigations show that retrieved quantities remain within usable limits for the majority of expected cirrus clouds. For example, for clouds with a lapse rate of 9 K km^{-1} and a linear absorption coefficient profile with gradient ranging from -2 to $+2$, optical depth can be retrieved to an accuracy of better than 20% and temperature to within 10 K of the midcloud temperature, for clouds of thickness 2 km or less and optical depths between 0.8 and 4.

1. Introduction

Cirrus clouds are recognized as a major and unique component in weather and climate research being relatively stable, long lived, present at all latitudes and seasons, and regularly covering ~20% of the globe (Liou 1986). However, much about them remains unresolved as they are hard to detect and identify via satellite and difficult to investigate in situ because of their high altitudes. They possess a wide range of radiative properties (Dowling and Radke 1990) but these are difficult to relate to their microphysical properties because of the theoretical problems involved in modeling nonspherical ice crystals. In the thermal infrared cirrus rarely have emissivities near unity (Ackerman et al. 1995) and even when completely opaque are not perfect radiators, reaching maximum monochromatic emissivities of only 0.95 (Liou 1974). Often, cirrus clouds are not opaque and transmit a significant amount of upwelling radiation and have emissivities that vary across the infrared atmospheric window (Ackerman et al. 1990).

Many retrievals using satellite data to determine cirrus cloud physical properties such as optical depth, particle size, and cloud temperature use measurements at two of more wavelengths and apply a theoretically or empirically derived relation between the differing radiative properties. Satellite data at 11- and 12-μm wavelengths are often used in this way for the retrieval of cirrus cloud temperature and infrared emissivity (e.g., Inoue 1985; Wu 1987; Parol et al. 1991; Lin and Coakley 1993). Measurements at either 11 or 12 μm have also been combined with 3.7-μm data (e.g., Lin and Coakley 1993; Ou et al. 1993, 1995), visible data (e.g., Minnis et al. 1993a,b), and data from the water vapor absorption channel at 6.5 μm (e.g., Szejwach 1982; Liou et al. 1990).

Prata and Barton (1993) proposed a retrieval of cirrus cloud optical depth utilizing the dual viewing facility of the Along-Track Scanning Radiometer (ATSR) instrument on the European Remote Sensing Satellite (*ERS-1*). Assumption of a nonscattering isothermal cloud allows the optical depth of the two views to be related, and thus a solution for cloud temperature (t_c) and optical depth (τ) at the 11- and 12-μm wavelengths is in theory possible without the need to relate the emissivities at the two wavelengths. In practice, it was found that for clouds with $0.6 < \tau < 10$ both cloud temperature and optical depth could be retrieved at each of the wavelengths using dual-angle dual-channel measurements; for optically thinner clouds, optical depth could be retrieved if independent knowledge of cloud temperature was available.

From simulations that included small uncertainties in cloud upwelling and exitant radiances, due, respectively, to the use of different atmospheric models and instru-

Corresponding author address: J. E. Russell, Space and Atmospheric Physics, Blackett Laboratory, Imperial College, London SW7 2BZ, United Kingdom.
E-mail: j.e.russell@ic.ac.uk

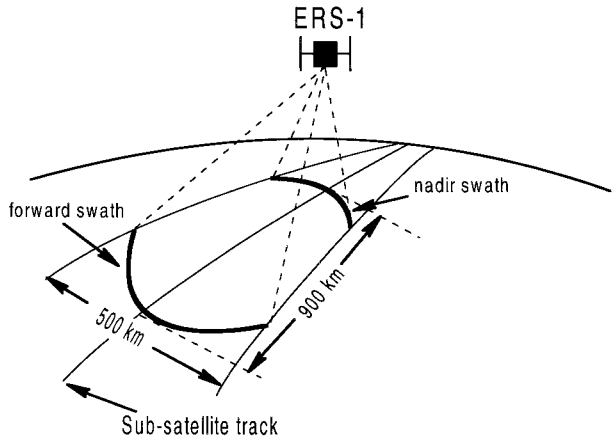

FIG. 1. Viewing arrangement of the ATSR instrument on the *ERS-1* satellite.

ment noise, Prata and Barton determined that retrieval of τ was possible to an accuracy of better than 15% for $0.1 < \tau_{\lambda=11\mu m} < 10$ and to better than 5% in the region $1 < \tau_{\lambda=11\mu m} < 6$. In their studies retrieved values were taken as an average of the values obtained assuming a range of model atmospheres and cloud heights. The simulated cloud exitant radiances were for isothermal nonscattering clouds with added measurement noise equivalent to the anticipated ATSR noise levels ($\approx$0.1 K NEΔT for a temperature of 220 K), which equates to less than a 0.3% difference in radiance.

2. The retrieval method

As the *ERS-1* satellite orbits the earth, the ATSR instrument views the surface using a conical scanning system. Every point on the surface is viewed first in a forward direction (approximately 55° to the local nadir), then about two minutes later at near nadir (see Fig. 1). If the contribution from the atmosphere above the cloud is assumed to be negligible, then for a nonscattering cirrus cloud with temperature t_c and optical depth τ, the satellite-observed nadir and forward exitant radiances ($R_{n,\lambda}$ and $R_{f,\lambda}$) may be expressed as

$$R_{n,\lambda} = e^{-\tau_\lambda \sec\phi_n} S_{n,\lambda} + (1 - e^{-\tau_\lambda \sec\phi_n}) B_\lambda(t_c), \quad (1)$$

$$R_{f,\lambda} = e^{-\tau_\lambda \sec\phi_f} S_{f,\lambda} + (1 - e^{-\tau_\lambda \sec\phi_f}) B_\lambda(t_c), \quad (2)$$

where $S_{n,\lambda}$ and $S_{f,\lambda}$ are the upwelling radiances incident at cloud base, and may be deduced either from satellite measurements of nearby cloud-free regions or from model atmosphere calculations. The subscripts n and f denote nadir and forward views, respectively; ϕ is the angle between the satellite viewing angle and the local vertical, along the subsatellite track $\phi_n \approx 0°$ and $\phi_f \approx 55°$. Because the cloud is assumed to be isothermal the radiating temperatures (t_c) in the forward and nadir cases are equal; thus, Eqs. (1) and (2) are nonlinear simultaneous equations with unknowns τ and t_c.

The effect on the retrieved cloud temperature and optical depth of small uncertainties on the upwelling and exitant radiances $S_{n,\lambda}$, $S_{f,\lambda}$, $R_{n,\lambda}$ and $R_{f,\lambda}$ was calculated using standard propagation of errors. Rearranging Eqs. (1) and (2) and substituting the transmission T_λ for $e^{-\tau_\lambda}$ we get

$$B_\lambda(t_c) = \frac{R_{n,\lambda} - T_\lambda^{\sec\phi_n} S_{n,\lambda}}{(1 - T_\lambda^{\sec\phi_n})}, \quad (3)$$

$$B_\lambda(t_c) = \frac{R_{f,\lambda} - T_\lambda^{\sec\phi_f} S_{f,\lambda}}{(1 - T_\lambda^{\sec\phi_f})}. \quad (4)$$

If Eq. (3) is denoted as g and Eq. (4) as h then, dropping the wavelength subscript for simplicity, f can be defined, for known constant values of ϕ_n and ϕ_f, as

$$f = g(R_n, S_n, T) - h(R_f, S_f, T) = 0. \quad (5)$$

For purposes of error analysis the uncertainty in the transmission σT can be deduced from the small uncertainties in the measured radiances when these uncertainties are independent of one another. From Eq. (5) using δT to represent the error in T, for a small uncertainty dT and similar notation for errors in the other quantities, we get

$$(\delta T)^2 = \frac{\left(\frac{\partial f}{\partial R_n}\right)^2 (\delta R)_n^2 + \left(\frac{\partial f}{\partial S_n}\right)^2 (\delta S)_n^2 + \left(\frac{\partial f}{\partial R_f}\right)^2 (\delta R_f)^2 + \left(\frac{\partial f}{\partial S_f}\right)^2 (\delta S_f)^2}{\left(\frac{\partial f}{\partial T}\right)^2}. \quad (6)$$

This can be simply converted to an uncertainty on τ by noting that

$$T = \exp(-\tau), \quad (7)$$

and thus

$$(\delta\tau)^2 = \left(-\frac{1}{T}\right)^2 (\delta T)^2. \quad (8)$$

Similarly, denoting $B(t_c)$ as B for simplicity,

$$B = g(R_n, S_n, T) = h(R_f, S_f, T). \quad (9)$$

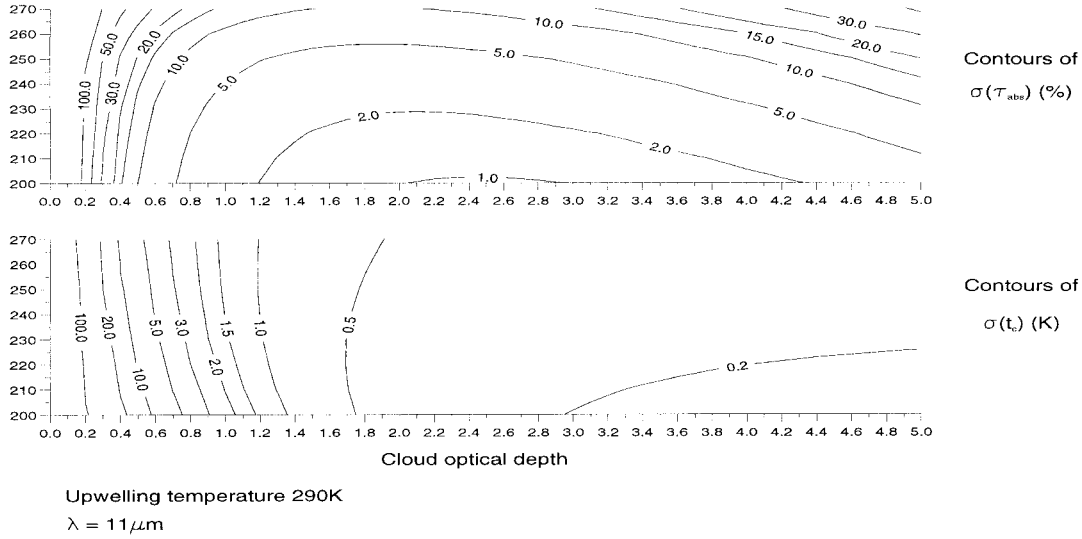

FIG. 2. Contours of uncertainty in the retrieved quantities as a function of cloud temperature for upwelling temperatures of 290 K, 0.5% uncertainty on forward and nadir upwelling and exitant radiances at a wavelength of 11 μm. (upper) Uncertainty in the retrieved cloud optical depth as a percentage of the true cloud optical depth; (lower) uncertainty in retrieved temperature (K).

Thus δB, the uncertainty in B, can be found from

$$(\delta B)^2 = \frac{\left(\frac{\partial g}{\partial R_n}\right)^2 (\delta R_n)^2 + \left(\frac{\partial g}{\partial S_n}\right)^2 (\delta S_n)^2 + \left(\alpha \frac{\partial h}{\partial R_f}\right)^2 (\delta R_f)^2 + \left(\alpha \frac{\partial h}{\partial S_f}\right)^2 (\delta S_f)^2}{\left(1 - \frac{\frac{\partial g}{\partial T}}{\frac{\partial h}{\partial T}}\right)^2}. \tag{10}$$

As t_c is related to B via the Plank function,

$$B = \frac{c_1 \upsilon^3}{\exp\left(\frac{c_2 \upsilon}{t_c}\right) - 1} \Delta\upsilon, \tag{11}$$

where c_1 and c_2 are constants, ν is the midchannel wavenumber, and $\Delta\nu$ is the channel width in wavenumbers, the error on t_c can be found from

$$(\delta t_c)^2 = \left[\frac{c_2 \upsilon}{B} - \frac{c_2 \upsilon}{c_1 \upsilon^3 \Delta\upsilon + B}\right]^2 \left[\ln\left(\frac{c_1 \upsilon^3 \Delta\upsilon}{B} + 1\right)\right]^{-4} (\delta B)^2. \tag{12}$$

Thus, for a given cloud temperature and optical depth and given upwelling radiances incident at cloud base, the cloud exitant radiance at chosen nadir and forward viewing angles can be determined at either 11 or 12 μm using Eqs. (1) and (2). The uncertainty on t_c and τ retrieved by this method can then be determined for given uncertainties on the upwelling and cloud exitant radiances by evaluating the partial differentials in Eqs. (8) and (12).

Such calclations indicate that the retrieval is slightly less sensitive to uncertainties in S and R at a wavelength of 11 μm than at 12 μm. For this reason the sensitivity results and the nonisothermal studies shown here are for a wavelength of 11 μm [ν = 923.25 cm^{-1}, $\delta\nu$ = 76.58 cm^{-1} in Eqs. (11) and (12) to correspond to the ATSR channel specifications; see Vass and Handoll (1991)]. Figures 2–5 show some results from the error calculations for a wavelength of 11 μm for cloud optical depths between 0.01 and 5. Figures 2, 4, and 5 are for upwelling radiances (S_n and S_f) corresponding to a brightness temperature of 290 K (upwelling temperature) and cloud temperatures between 200 and 270 K. Figure 3 is for a cloud temperature of 213 K and up-

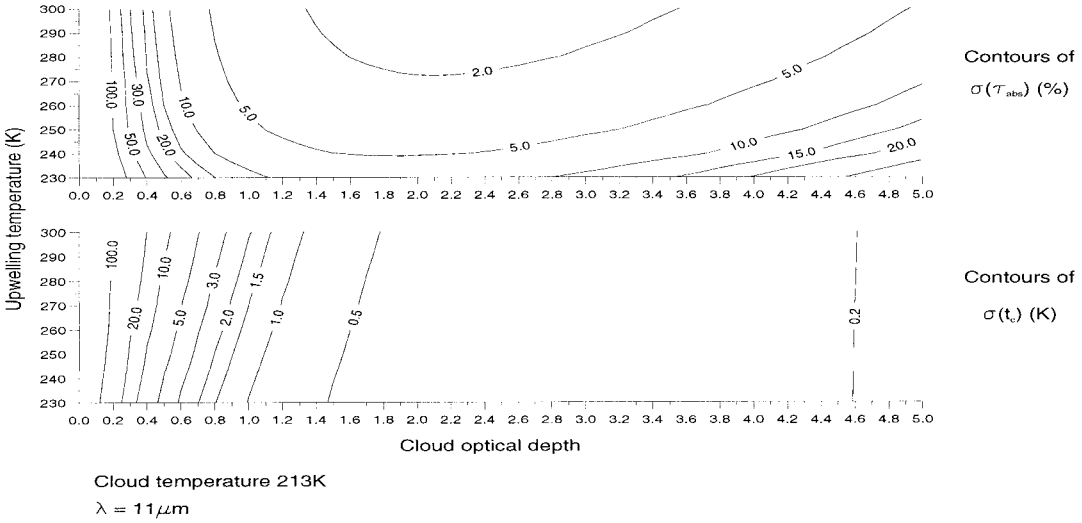

FIG. 3. As in Fig. 2 but showing the effect of upwelling temperature for a constant cloud temperature of 213 K.

welling temperatures between 230 and 300 K. The cloud exitant radiances (R_n and R_f) were calculated for a nonscattering homogeneous cloud using Eqs. (1) and (2) with $\phi_n = 0$ and $\phi_f = 55°$. The forward and nadir upwelling temperatures were assumed to be equal and the effect of the atmosphere above the cloud was assumed negligible. In reality, small differences are expected between the nadir and forward upwelling temperatures due to the different path lengths through the atmosphere for the two views. In order to test the sensitivity of these results to differences between the upwelling temperatures, the calculations were repeated using a forward upwelling temperature 2 K less than the nadir. This difference is double that expected between viewing angles 0° and 55° for a cloud at the tropopause within a *U.S. Standard Atmosphere* profile. There was a negligible difference between these results for unequal upwelling temperatures and those presented here for equal forward and nadir upwelling temperatures.

The sensitivity of the retrieved quantities to 0.5% uncertainties on upwelling and exitant radiances, approximately equivalent to expected noise-level errors, is shown as a function of cloud temperature for a fixed upwelling temperature of 290 K in Fig. 2 and as a function of upwelling temperature, for a cloud temperature of 213 K, in Fig. 3. In each of these figures for a given cloud and upwelling temperature the error in τ decreases with increasing optical depth to a minimum value at an optical depth between 1.5 and 2.5, it then increases when cloud optical depth is further increased. However, the error in t_c continually decreases with increasing cloud optical depth. For both quantities, errors are large at low optical depths as the cloud exitant radiance consists mainly of transmitted upwelling radiance; therefore, little cloud information is present. Errors in τ increase beyond a critical optical depth because its retrieval relies on different information from the two views. In the limit of very optically thick clouds, transmitting an insignificant amount of upwelling radiation, the forward and nadir radiances become equal and contain no information on τ. Conversely, for these optically thick clouds information on cloud temperature is maximized; thus the errors in t_c decrease with increasing optical depth.

Comparison of Figs. 2 and 3 also indicates that the error in τ is a strong function of the difference between the cloud temperature and upwelling temperature (the cloud–upwelling contrast), whereas this difference has only a slight effect on the retrieved t_c. Large values of the cloud–upwelling contrast allow retrieval of τ to a higher degree of accuracy over an optimum optical depth range than is possible at lower contrasts.

The lesser effect of the cloud–upwelling contrast on the retrieved t_c can be attributed to the opposing effects of contrast on this quantity. Greater contrast leads to a better determination of τ and hence of t_c. Conversely, at lower contrasts a given error in τ leading to an error in the separation of the exitant radiance into upwelling and cloud contributions results in a smaller difference to the retrieved t_c because of the similarity between cloud and upwelling temperatures. Thus, at low optical depths where the transmitted portion of the upwelling radiation is dominant in the exitant radiance, an increase in contrast leads to a slight increase in the uncertainty in the retrieved cloud temperature at a given cloud optical depth. However, as the cloud optical depth increases, the contribution to the exitant signal from the cloud becomes more dominant. Thus, at larger optical depths the retrieval of cloud temperature becomes more accurate for high cloud–upwelling contrasts for which the optical depth is also more accurately determined.

Figures 4 and 5 show the errors in the retrieved quantities for 2.0% uncertainties on the upwelling radiances with 0.5% uncertainties on the exitant radiances and for 2.0% uncertainties on the exitant radiances with 0.5%

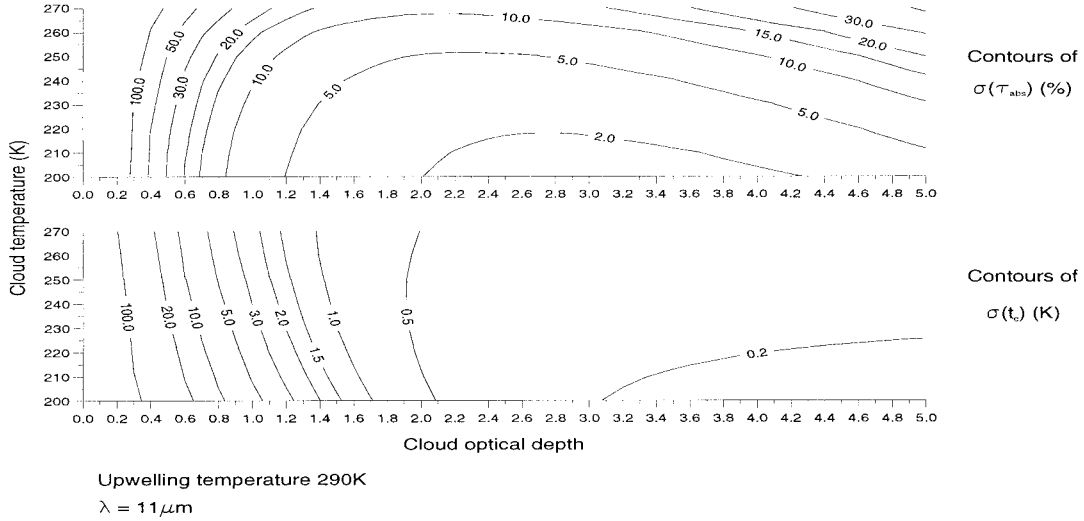

FIG. 4. As in Fig. 2 but for 2% uncertainty on upwelling radiance and 0.5% uncertainty on exitant radiances.

uncertainties on the upwelling radiances, respectively. The results allow the relative sensitivity of the retrieval to uncertainties in the upwelling and exitant radiances to be compared. They clearly show that the retrieved quantities are more sensitive to uncertainties in the exitant radiances than to uncertainties in the upwelling radiances. Compared to Fig. 2, Fig. 4 indicates that the increase of uncertainty in upwelling radiance, from 0.5% to 2%, has the greatest effect on the retrieved quantities for clouds with low optical depths. This is because the upwelling component of the exitant radiance is most significant at low optical depths and decreases as optical depth increases. Thus, for $\tau > 5$ the difference between the errors shown in Fig. 4 and those shown in Fig. 2 are negligible. Comparing Figs. 2 and 5 we see that increasing the uncertainty on the exitant radiance causes significant increase to the errors in the retrieved quantities at all optical depths. In this case the effect is greatest at larger optical depths where the cloud portion of the exitant radiance is most significant.

In reality, cirrus clouds are not isothermal, homogeneous, and nonscattering, and these assumptions will produce further uncertainties in the retrieved quantities. Our investigations (not shown here) using a range of different distributions, both measured in situ and defined by previous authors (e.g., Takano and Liou 1989), have shown that scattering generally has a much smaller effect on the retrieval than cloud vertical inhomogeneity. These studies showed that scattering within a cirrus cloud reduces the cloud exitant radiance by an amount that varies with optical depth and with particle size and shape (Russell 1996; Russell et al. 1997). For an iso-

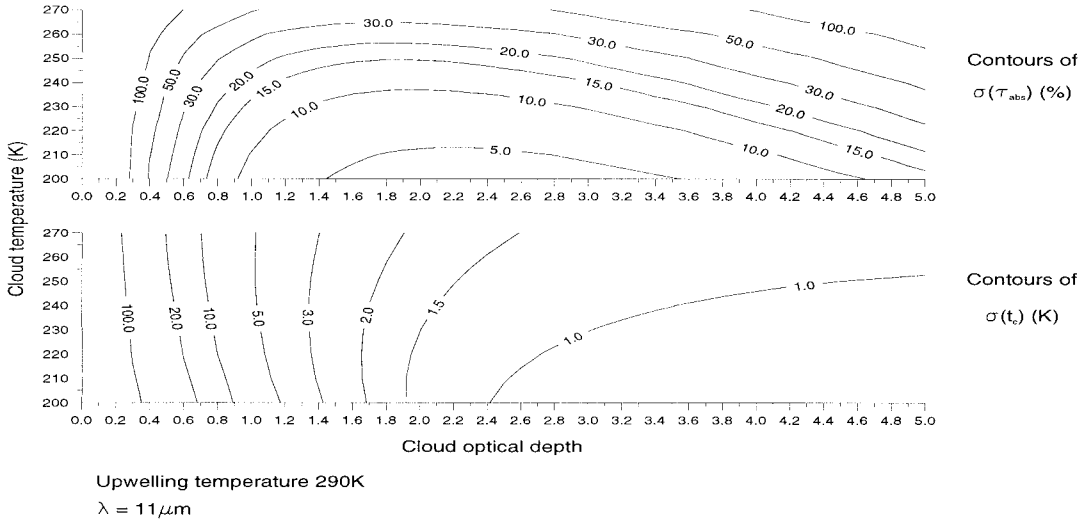

FIG. 5. As in Fig. 2 but for 0.5% uncertainty on upwelling radiances and 2% uncertainty on exitant radiances.

thermal scattering cirrus cloud at a wavelength of 11 μm with an absorption optical depth $1.0 < \tau < 5.0$, the error in the retrieved temperature was less than errors shown here for nonisothermal clouds with thicknesses greater than 0.5 km for all the particle distributions used. For the majority of distributions, the same was true for the error in the retrieved optical depth. For a few cases, errors in the retrieved optical depth reached values as large as those shown here for nonisothermal clouds with thicknesses of about 3 km. However, the optical depths and the particle number concentrations of the distributions for which these errors occurred necessitated cloud thickness much greater than 3 km. Therefore, when scattering and nonisothermal effects are considered for these clouds, nonisothermal effects dominate. For exceptional cirrus clouds, which have a small vertical extent, small particles sizes, and absorption optical depths between 2.0 and 2.5 at 11 μm, scattering may produce errors greater than those due to nonisothermal effects. However, for most cirrus clouds, nonisothermal effects are expected to dominate the errors due to scattering.

The results of investigations into the impact of cloud vertical inhomogeneity on the retrieval are presented in section 3. Uncertainties in the upwelling radiances are not included and additional noise has not been added to the exitant radiances from the nonisothermal clouds. This allows the effects of vertical inhomogeneity to be studied in isolation and means that the differences shown are purely bias errors due to a breakdown of the assumptions in the retrieval.

The sensitivity results in this section are used as a guide when determining the significance of the errors caused by vertical inhomogeneity within the cloud. In particular Fig. 2, showing the sensitivity of the retrieved quantities to 0.5% uncertainties on the upwelling and exitant radiances, is used as a comparison. These errors are referred to as the ''minimum uncertainties'' of the retrieval as they approximately correspond to expected signal noise and can therefore be considered the best possible determination of the parameters using this method.

3. The effect of vertical inhomogeneity

For a nonscattering vertically inhomogeneous cloud, where $z = 0$ at cloud base and Δz at cloud top, the exitant radiance at any view angle ϕ can be expressed as

$$R_\phi = S_\phi \exp\left[-\int_{z=0}^{z=\Delta z} k_{\text{abs}}(z)\,\sec\phi\,dz\right] + \int_{z=0}^{z=\Delta z} k_{\text{abs}}(z)B[t_c(z)] \times \exp\left[-\int_{z'=z}^{z'=\Delta z} k_{\text{abs}}(z)\,\sec\phi\,dz'\right]\sec\phi\,dz, \quad (13)$$

where k_{abs} is the absorption coefficient and the total optical depth of the cloud (τ) is defined as

$$\tau = \int_{z=0}^{z=\Delta z} k_{\text{abs}}(z)\,dz. \quad (14)$$

Thus, the exitant radiance is dependent on the particular form of the absorption coefficient profile $k_{\text{abs}}(z)$ as well as the temperature profile $t_c(z)$.

The second term in Eq. (13) can be represented by the equivalent term for an isothermal cloud of the same optical depth: $(1 - e^{-\tau})B(t_c')$; this defines t_c', the ''radiating temperature'' of the nonisothermal cloud, or

$$B(t_c') = \frac{R_\phi - S_\phi\, e^{-\tau\sec\phi}}{1 - e^{-\tau\sec\phi}} = \frac{\displaystyle\int_{z=0}^{z=\Delta z} k_{\text{abs}}(z)B[t_c(z)]\exp\left[-\int_{z'=0}^{z'=\Delta z} k_{\text{abs}}(z')\,\sec\phi\,dz\right]\sec\phi\,dz}{1 - e^{\tau\sec\phi}}, \quad (15)$$

where t_c' can be considered as the weighted mean temperature of the cloud, where the weightings are determined by the line-of-sight transmission gradients. For an isothermal cloud $t_c' = t_c$, independent of the view angle, but for a nonisothermal cloud t_c' will be a function of view angle and will depend on the vertical distribution of the temperature and absorption properties.

Calculations were carried out for a range of assumptions concerning the variation of absorption coefficient with height. The total particle cross section, determined from aircraft data collected during the European Cloud and Radiation Experiment 1993 (EUCREX '93) campaign, was used in conjunction with previously published observations to aid in the development of physically justifiable absorption coefficient profiles. From inspection of the EUCREX '93 data, linearly increasing with altitude, and quadratically peaked k_{abs} profiles with gradients between 0 and 2 were used (Russell 1996). Previous studies (e.g., Smith et al. 1990; Heymsfield et al. 1990; Kinne et al. 1992) of cirrus clouds observed total particle cross section or ice water content being approximately constant or decreasing with increasing altitude or temperature. Therefore, linearly decreasing k_{abs} profiles were also

TABLE 1. The properties for constant, linear, and peaked absorption coefficient profiles used.

	Constant k_{abs}	Linear k_{abs}	Peaked k_{abs}
k_{abs} profile	$k_{abs} = c$	$k_{abs} = mz + c$	$k_{abs} = -m\left(z - \frac{\Delta z}{2}\right)^2 + c$
τ_0	$c\Delta z$	$\frac{m(\Delta z)^2}{2} + c\Delta z$	$-\frac{m(\Delta z)^3}{12} + c\Delta z$
c	$\frac{\tau}{\Delta z}$	$\frac{\tau}{\Delta z} - \frac{m\Delta z}{2}$	$\frac{\tau}{\Delta z} + \frac{m(\Delta z)^2}{12}$
$k_{abs}(z)$	$\frac{\tau}{\Delta z}$	$mz + \frac{\tau}{\Delta z} - \frac{m\Delta z}{2}$	$-m\left(z - \frac{\Delta z}{2}\right)^2 + \frac{\tau}{\Delta z} + \frac{m(\Delta z)^2}{12}$
$\tau(z)$	$\tau - z\frac{\tau}{\Delta z}$	$\tau - z\left(\frac{mz}{2} + \frac{\tau}{\Delta z} - \frac{m\Delta z}{2}\right)$	$\tau - z\left[\frac{\tau}{\Delta z} + \frac{m(\Delta z)^2}{12}\right] + m\left[\frac{z^3}{3} - \frac{z^2\Delta z}{2} + \frac{z(\Delta z)^2}{4}\right]$
Physical region	$\tau \geq 0$	$\tau \geq \frac{\lvert m\rvert(\Delta z)^2}{2}$	$\tau \geq \frac{m(\Delta z)^3}{6}$

included in the studies presented below. As no other information was available, gradients identical to those used for the linearly increasing cases were used for the linearly decreasing profiles.

For each study the cloud was divided into N nonscattering layers of equal geometric thickness that were each assumed isothermal, where the temperature difference across a layer was less than 0.1 K. The temperature of each layer was assigned assuming a uniform temperature lapse rate through the cloud, and the optical depth of each layer was calculated from its thickness and absorption coefficient. The radiance leaving the top of a layer in the nadir and forward directions was calculated from Eqs. (1) and (2) with the upwelling radiances equal to that leaving the top of the underlying layer.

For the first study the absorption coefficient was kept constant with height; in the second study the absorption coefficient was considered to be a linear function of height,

$$k_{abs} = mz + c, \tag{16}$$

where m is the gradient of the k_{abs} profile; and c is determined by the cloud thickness Δz and optical depth τ,

$$c = \frac{\tau}{\Delta z} - \frac{m\Delta z}{2}. \tag{17}$$

Values of $m = \pm 1.0$ and ± 2.0 were used. In this case physically reasonable values of the absorption coefficient require

$$\tau \geq \frac{|m|(\Delta z)^2}{2}. \tag{18}$$

For the third study the absorption coefficient was taken as a quadratically peaked function of height, with a maximum value at midcloud; thus

$$k_{abs} = -m\left(z - \frac{\Delta z}{2}\right)^2 + c, \tag{19}$$

with z defined as before and m taking values of 1.0, and 2.0 and

$$c = \frac{\tau}{\Delta z} + \frac{m(\Delta z)^2}{12}. \tag{20}$$

In this case the condition for $k_{abs} \geq 0$ for positive m is

$$\tau \geq \frac{m(\Delta z)^3}{6}. \tag{21}$$

The properties of the different types of absorption coefficient used are summarized in Table 1.

The exitant radiance was calculated at viewing angles of 0° and 55° for different values of cloud thickness and optical depth for each of the k_{abs} profiles. The results were then used in conjunction with the upwelling radiances as input to the isothermal nonscattering retrieval. The cloud optical depth and temperature retrieved by this method were then compared with the optical depth and midcloud temperature used to generate the exitant radiances. Investigations of this nature were carried out for clouds with geometrical thickness ranging from 0.1 to 5 km and optical depths from 0.1 to 5.0.

For these studies a midcloud temperature of 233 K and forward and nadir upwelling temperatures of 290 K were used. Lapse rates of between 4 and 10 K km^{-1} have been recorded in cirrus clouds by Ansmann et al. (1993), who in a study of 38 cirrus clouds found that around 74% had lapse rates between 7 and 9 K km^{-1}. The results shown here are for a lapse rate of 9 K km^{-1}; this represents the worst likely scenario and is close to the dry-adiabatic lapse rate, which is appropriate for conditions relatively high in the troposphere. Extension of the results to clouds with different temperature lapse rates is discussed at the end of section 3.

a. Impact on radiating temperature

As the retrieval assumes an isothermal cloud, careful consideration was given to how the retrieved temper-

ature should be compared to the ''actual'' cloud temperature. Cloud-radiating temperature might be seen as the most natural comparison, but as Eq. (15) shows, for a nonisothermal cloud this depends on view angle ϕ, and thus differs between the forward and nadir views. Comparison with a temperature at a fixed location within the cloud would therefore be preferable, as this would be invariant with view angle. Cloud-top temperature is often stated as a required quantity but it is only of real relevance for optically thick clouds. For semitransparent cloud, where transmitted radiation is a significant component of the exitant cloud radiance, radiation from the whole depth of the cloud contributes to the signal. Thus, for these studies, comparison of the retrieved temperature to midcloud temperature was considered better than a comparison to either the cloud-top or radiating temperatures. Therefore, the discussion of the error in the retrieved temperature is concerned with the difference between the retrieved and midcloud temperatures. To give an idea of the relationship between the retrieved temperature and a cloud-radiating temperature, the difference between the retrieved temperature and the nadir cloud-radiating temperature is also shown.

The effect of vertical inhomogeneity within the cloud means that the assumption that the forward- and nadir-radiating temperatures are equal in Eqs. (1) and (2) is no longer valid. The forward view through a cloud with optical depth τ, thickness Δz, lapse rate Γ, and absorption coefficient profile of gradient m ''experiences'' a cloud with optical depth, cloud thickness, and lapse rate of $\sec\phi\tau$, $\sec\phi\Delta z$, and $\Gamma/\sec\phi$ respectively. The gradient of the absorption coefficient profile experienced by the forward view is $m/\sec\phi$ for the linear cases and is $m/(\sec\phi)^{1/2}$ for the quadratically peaked profiles. These differences lead to the differences in the radiating temperature between the forward and nadir views.

The magnitude of the effect on the retrieved quantities is a combination of the difference between the radiating temperatures (see Fig. 6b) and the sensitivity of the retrieval (Fig. 3). In the case of the retrieved temperature, the difference between the cloud-radiating and the midcloud temperature (Fig. 6a) also contributes to the difference between the retrieved and the actual midcloud temperatures. Thus, the variation of the difference between the nadir and forward cloud-radiating temperatures and between the nadir-radiating temperature and the midcloud temperature, as a function of optical depth and cloud thickness for the different absorption coefficient profiles, indicates the relative importance of these factors on the accuracy of the retrieval.

Calculations were made for each of the chosen absorption coefficient profiles for vertically inhomogeneous clouds of different thicknesses with lapse rates of 9 K km^{-1}. Figures 6(i)–(iii) show the variation of (a) the nadir-radiating temperature t_c' and (b) the difference between the nadir- and forward-radiating temperatures, $\Delta t_c'$, as a function of cloud optical depth. From Figs. 6a(i)–(iii) it can be seen that, except for the linearly increasing profile at very low optical depths, t_c' becomes warmer with decreasing optical depth. As $\tau \to 0$, t_c' for the constant k_{abs} cloud tends to the midcloud temperature; whereas for linearly increasing and linearly decreasing profiles t_c' tends toward top and bottom temperatures, respectively. This is because as $\tau \to 0$ the dominant contributions to t_c' come from the region of largest absorption coefficient, that is, cloud top for the linearly increasing k_{abs} and cloud base for the linearly decreasing profile. As $\tau \to \infty$, t_c' for all the profiles tends to the cloud-top temperature. Thus, the radiating temperature decreases most steeply for the $m = -2$ profile and least steeply for the $m = 2$ profile. As the cloud thickness increases, the difference between the t_c' for different profiles also increases.

From Figs. 6b(i)–(iii) it is seen that the difference between the forward- and nadir-radiating temperatures, $\Delta t_c'$, is a peaked function of optical depth that tends to zero in the limits of optically thin and optically thick clouds. For nearly transparent clouds, the contribution from all layers is hardly affected by the difference in pathlength between the two views; as the cloud becomes increasingly more opaque, nadir- and forward-radiating temperatures both tend toward the cloud-top temperature. Between these two extremes the extra pathlength through the cloud in the forward view results in a ''limb-darkening effect,'' whereby the forward-radiating temperature corresponds to a higher and therefore colder level in the cloud than the nadir.

As cloud thickness increases, $\Delta t_c'$ increases for a given profile and cloud optical depth. The relationship between $\Delta t_c'$ for the different profiles also changes. Increasing the cloud thickness does not alter the position of the peak for the constant k_{abs} cloud but causes the peaks for the clouds with varying k_{abs} profiles to shift to progressively higher optical depths. We may therefore expect the effect of increasing cloud thickness to produce a regular increase in the errors in the retrieved quantities for the constant absorption coefficient case, whereas for the other profiles the rate of increase of the errors with increasing cloud thickness depends on the cloud optical depth.

For a given optical depth and cloud thickness, $\Delta t_c'$ is greater for the constant k_{abs} profile than for the quadratically peaked profiles or the linearly increasing profiles. At low optical depths $\Delta t_c'$ is less for the linearly decreasing profiles than for the constant k_{abs} profile, while the reverse is true at larger optical depths; thus the curves of the linearly decreasing profiles cross the curves for the constant k_{abs} clouds at an optical depth that increases with increasing cloud thickness. Therefore, at all optical depths the effect of vertical inhomogeneity on the retrieval will be greater for the constant k_{abs} clouds than for clouds with linearly increasing and quadratically peaked k_{abs} profiles. At low optical depths the effect for the constant k_{abs} cloud will also be greater than that of the linearly decreasing k_{abs} profile, but the reverse will be true for these two profiles at large

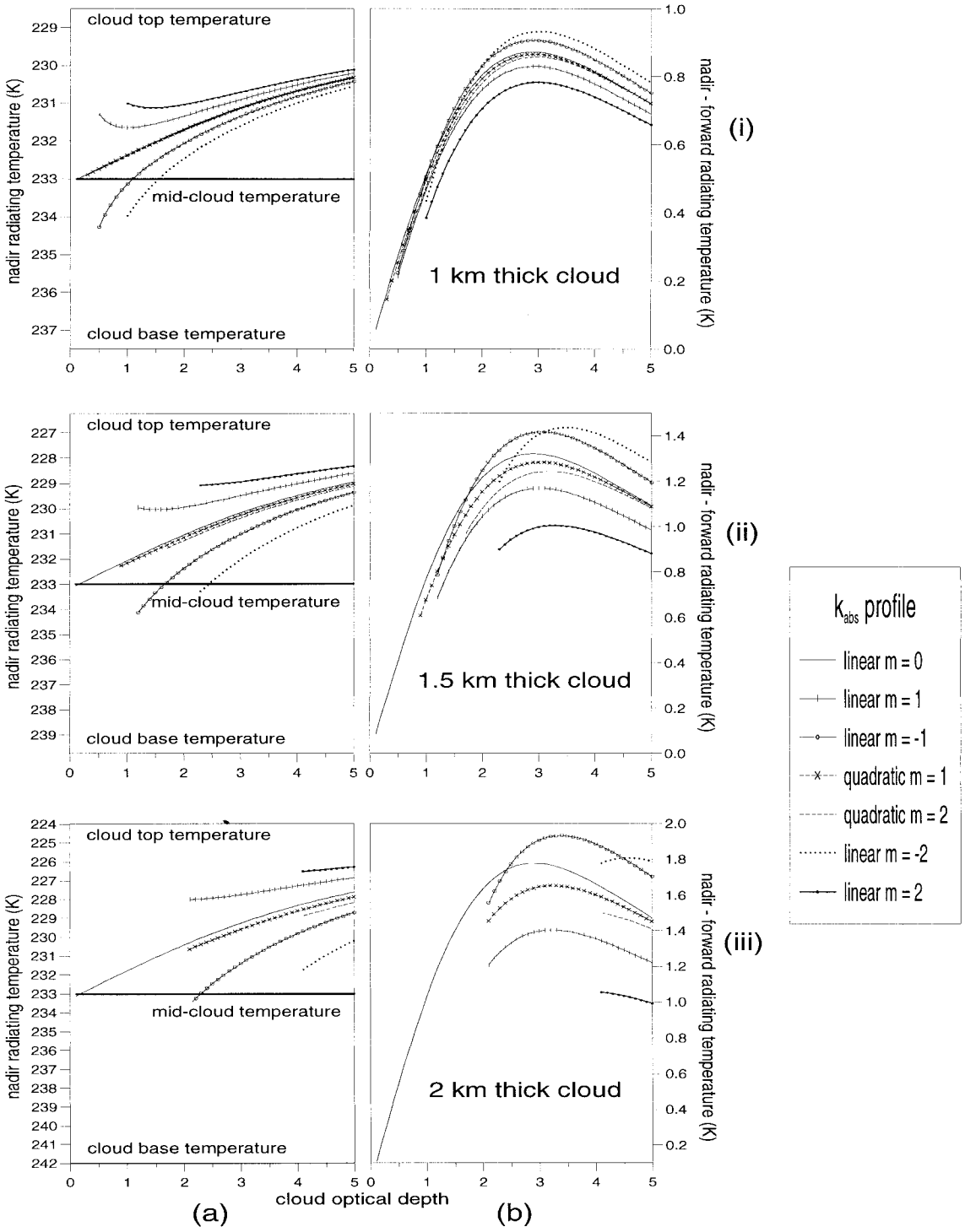

FIG. 6. (a) (left) Nadir-radiating temperature and (b) (right) nadir-minus forward cloud-radiating temperature; as a function of cloud optical depth for (i) 1.0-, (ii) 1.5-, and (iii) 2.0-km thick vertically inhomogeneous clouds with temperature lapse rates of 9 K km^{-1} and different absorption coefficient profiles.

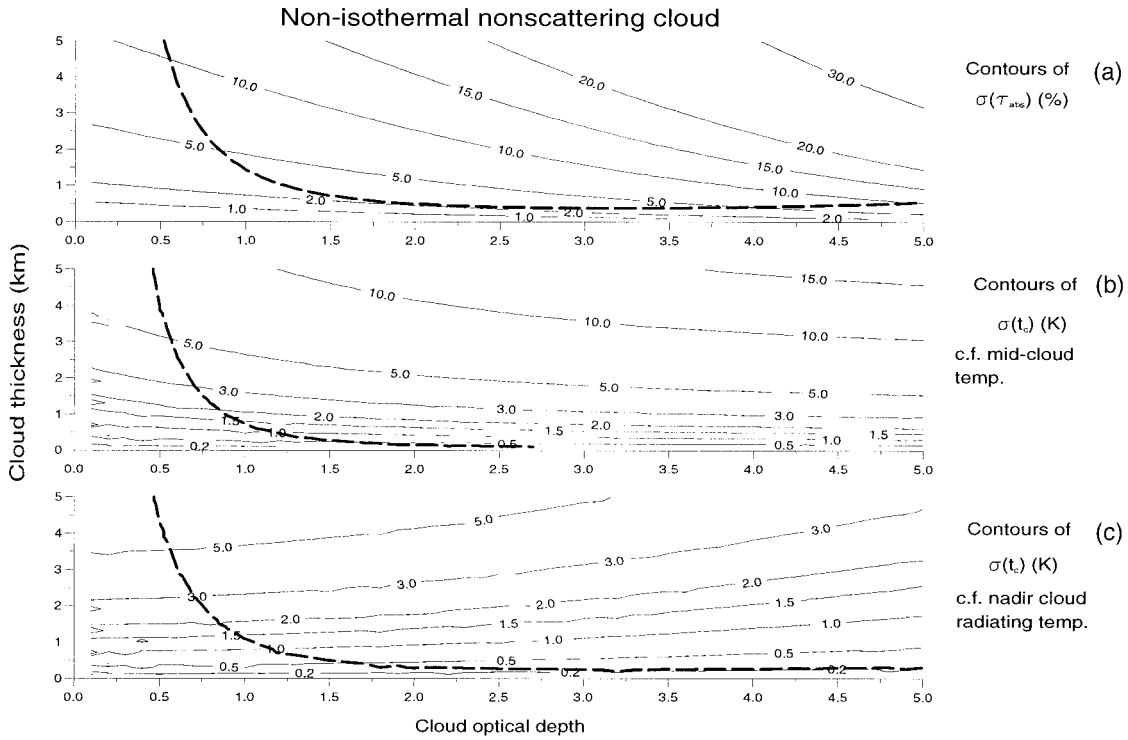

FIG. 7. Contours of error in the retrieved quantities when exitant radiances from a nonscattering nonisothermal cloud with a constant absorption coefficient are used as input to the retrieval. (a) Difference between the actual and retrieved optical depth (%); (b), (c) actual cloud temperature minus retrieved temperature. (b) Actual cloud temperature is taken to be the midcloud temperature; (c) actual cloud temperature is taken to be the nadir cloud-radiating temperatures. Calculations were performed at a wavelength of 11 μm using an upwelling temperature of 290 K for a cloud with a midtemperature of 233 K and a constant temperature lapse rate of 9 K km^{-1}.

optical depths. The effect of vertical inhomogeneity on the retrieved optical depth and cloud temperature is discussed in more detail below.

b. Impact on the retrieved quantities

The differences between the forward- and nadir-radiating temperatures (see Fig. 6b), for the absorption coefficient profiles investigated here, indicate that clouds with peaked or increasing k_{abs} will, for a given cloud thickness and optical depth, produce smaller errors in the retrieved optical depth than clouds with constant k_{abs} under all conditions. Similarly, larger errors are expected for clouds with decreasing k_{abs} profiles than for those with constant k_{abs}, except at low optical depths.

The variation of the nadir-radiating temperature with optical depth and cloud thickness shown in Fig. 6a for the different k_{abs} profiles indicates that differences between the midcloud and cloud-radiating temperatures increase with increasing optical depth and with increasing cloud thickness. Therefore, errors in the retrieved cloud temperature measured with respect to the midcloud temperature may also be expected to be affected in this manner.

For the k_{abs} profiles investigated, the difference between the error in the retrieved quantities for clouds with constant k_{abs} and those with varying k_{abs} was found to be within the range $+3.5\%$ to 6.0% in $\sigma(\tau)$ and $+2$ to -4 K in $\sigma(t_c)$ (for $\Delta z \leq 5$ km and $\tau \leq 4$). Thus, the use of a constant k_{abs} was considered a fairly good approximation. For this reason the errors in the retrieved quantities due to vertical temperature inhomogeneity are discussed below only for the constant k_{abs} situation.

Figure 7 shows the errors in the retrieved quantities that result when the retrieval uses input generated for upwelling forward and nadir radiances equal to that of a blackbody at 290 K incident on a nonscattering vertically inhomogeneous cloud with an actual midcloud temperature of 233 K and a temperature lapse rate of 9 K km^{-1} [see Eq. (13)]. Figure 7a shows $\sigma(\tau)$, which is the percentage difference between the retrieved and actual optical depth, while Figs. 7b,c show $\sigma(t_c)$, the difference in kelvins between the retrieved temperature and actual cloud temperature. For Fig. 7b the actual cloud temperature is taken to be the midcloud temperature and for Fig. 7c the actual cloud temperature is taken to be the nadir cloud-radiating temperature as defined in Eq. (15). Positive values of $\sigma(\tau)$ and $\sigma(t_c)$ indicate that the retrieved quantities were less than the actual values.

These results shown in Fig. 7 do not include the effect of additional noise on either the upwelling or the cloud exitant radiances. For this reason the heavy dashed black

line in Fig. 7 indicates how the errors shown here compare with the minimum uncertainties (see section 2): to the bottom left of this line, minimum uncertainties as determined in Figs. 2 and 3 are larger than the errors shown here; in the remainder of plot, above and to the right of the line, the plotted errors are larger than the minimum uncertainties of the method. From the position of this line it can be seen that over the range of cloud thickness and optical depth shown, the majority of errors are greater than the minimum uncertainties of the method. For example, from Fig. 7 it can be seen that nonisothermal clouds thicker than 1 km with a constant absorption coefficient produce errors in the retrieved temperature greater than minimum uncertainties when $\tau \lesssim 0.7$ and in the retrieved optical depth for $\Delta z > 1.0$ km and $\tau > 1.0$.

The structure of $\sigma(\tau)$ shown in Fig. 7a is a combination of the difference between the nadir- and forward-radiating temperatures ($\Delta t_c'$) shown in Figs. 6b(i)–(iii) and the sensitivity of the method as indicated in Fig. 2. The combination of the largest $\Delta t_c'$ in the midoptical depth range, where the sensitivity of the method is smallest with smaller $\Delta t_c'$ at larger and smaller optical depths, where the retrieval is more sensitive, leads to a smooth variation in $\sigma(\tau)$ with optical depth. The structure of $\sigma(t_c)$ shown in Figs. 7b,c is due to the difference between the forward- and nadir-radiating temperatures, the sensitivity of the method. For Fig. 7b, $\sigma(t_c)$ is also affected by the difference between midcloud and cloud-radiating temperatures. Thus, at high optical depths, as the cloud-radiating temperature tends to the cloud-top temperature, despite the fact that both $\Delta t_c'$ and the sensitivity of the retrieved temperature to small uncertainties decrease, $\sigma(t_c)$ in Fig. 7b continues to increase, tending toward the difference between midcloud and cloud-top temperatures.

These results can be extended to clouds with different temperature lapse rates. The temperature difference through the cloud is the factor responsible for the nonisothermal effects; this is a combination of the temperature lapse rate within the cloud and the cloud thickness. Thus, for the constant absorption coefficient case the results for different temperature lapse rates can be derived quite simply from the results shown in Fig. 7 by suitable adjustment of the cloud thickness axis. For example, a cloud with a lapse rate of 4.5 K km^{-1} would result in a graph similar to Fig. 7 except the values on the cloud thickness axes would be doubled. Therefore, a 2-km thick cloud with a lapse rate of 4.5 K km^{-1} would have the same temperature difference and thus the same exitant radiance and errors in retrieved quantities as a 1-km thick cloud with a lapse rate of 9 K km^{-1}.

4. Summary and conclusions

Vertical inhomogeneity has a significant influence on the accuracy of the cloud temperature and optical depth retrieved from dual-angle infrared measurements if an isothermal cloud is assumed. Over most of the range of cloud optical depth and geometrical thickness investigated here, errors in the optical depth and cloud temperature due to cloud vertical inhomogeneity are greater than the minimum uncertainties of the method and than the errors suggested by Prata and Barton (1993).

Vertically inhomogeneous clouds result in the breakdown of the assumption that the cloud temperature is equal in forward and nadir views. The magnitude of the effect is determined by the difference between the nadir and forward cloud-radiating temperatures. For a constant absorption coefficient profile this difference increases regularly with increasing cloud thickness and with an increase in the temperature lapse rate within the cloud. The exact form of the absorption coefficient profile also affects the difference between the forward- and nadir-radiating temperatures.

However, over the range of conditions investigated here, the exact manner in which the absorption coefficient varies within a cloud is seen to be a second-order effect compared with the effect of the expected temperature variations within the cloud. The results for the constant absorption coefficient case can therefore be considered a reasonable, simple approximation to the errors in the retrieved quantities due to cloud vertical inhomogeneity. The errors for the other profiles investigated here are within $+3.5\%$ to -6.0% for $\sigma(\tau)$ and $+2$ to -4 K for $\sigma(t_c)$ of the errors shown for the constant absorption coefficient profile for $\Delta z \leq 5$ km and $\tau \leq 4.0$ when a temperature lapse rate of 9 K km^{-1} is used.

From these results it can be seen that although the errors in the retrieved temperature and optical depth are considerably greater than the noise-level errors and than the errors estimated by Prata and Barton (1993), they remain within useful limits for the majority of expected cloud cases. For example, for the constant absorption coefficient cloud with a temperature lapse rate of 9 K km^{-1} at an average cirrus cloud thickness of 1.5 km (Dowling and Radke 1990) for $0.8 < \tau < 4.0$, errors are less than 15% in the retrieved optical depth and less than 5 K in retrieved temperature. For clouds less than 2 km thick ($\sim$70% of recorded cases; see Dowling and Radke 1990), errors are less than 18% in the retrieved optical depth and less than 7 K in retrieved temperature for $0.8 < \tau < 4.0$. As these errors are due to the temperature difference through the cloud, the results shown in Fig. 7 can easily be adjusted for different temperature lapse rates by appropriate adjustment of the cloud thickness axis.

This work demonstrates the importance of considering the vertical temperature structure of a semitransparent cirrus cloud when determining the uncertainty of quantities retrieved from thermal infrared data. Although the study considered a dual-angle retrieval, nonisothermal effects will also result in inaccuracies for dual-wavelength retrievals that assume isothermal

clouds. The importance of this effect will vary with the wavelength combinations being used and with the microphysical properties of the cloud. This work also indicates that nonisothermal effects within cirrus should be taken into consideration when using cloud temperatures retrieved from either dual-angle or multiwavelength data. For most cirrus clouds, which are optically thin in the infrared, the retrieved temperature cannot be considered to represent the cloud-top temperature but will correspond to deeper layers within the cloud. The level of the cloud to which the retrieved temperature corresponds will vary according to the cloud optical depth and vertical structure.

Acknowledgments. This research was funded by a Gassiot grant from the U.K. Meteorological Office. The EUCREX '93 data used for this work was supplied by Peter Francis from Met Research Flight.

REFERENCES

Ackerman, S. A., W. L. Smith, J. D. Spinhirne, and H. E. Revercomb, 1990: The 27–28 October 1986 FIRE IFO cirrus case study: Spectral properties of cirrus clouds in the 8–12 μm window. *Mon. Wea. Rev.,* **118,** 2377–2388.

——, ——, A. D. Collare, X. L. Ma, H. E. Revercomb, and R. O. Knuteson, 1995: Cirrus cloud properties derived from high spectral resolution infrared spectrometry during FIRE II. Part II: Aircraft HIS results. *J. Atmos. Sci.,* **52,** 4246–4263.

Ansmann, A., and Coauthors, 1993: Lidar network observations of cirrus morphological and scattering properties during the International Cirrus Experiment 1989: The 18 October 1989 case study and statistical analysis. *J. Appl. Meteor.,* **32,** 1608–1622.

Dowling, D. R., and L. F. Radke, 1990: A summary of the physical properties of cirrus clouds. *J. Appl. Meteor.,* **29,** 970–978.

Heymsfield, A. J., K. M. Miller, and J. D. Spinhirne, 1990: The 27–28 October 1986 FIRE IFO cirrus case study: Cloud microstructure. *Mon. Wea Rev.,* **118,** 2313–2328.

Inoue, T., 1985: On the temperature and effective emissivity determination of semi-transparent cirrus clouds by bi-spectral measurements in the 10 μm window region. *J. Meteor. Soc. Japan,* **63,** 88–98.

Kinne, S., T. P. Ackerman, A. J. Heymsfield, F. P. J. Valero, K. Sassen, and J. D. Spinhirne, 1992: Cirrus microphysics and radiative transfer: Cloud field study on 28 October 1986. *Mon. Wea. Rev.,* **120,** 661–684.

Lin, X., and J. A. Coakley, 1993: Retrieval of properties for semi-transparent clouds from multispectral infrared imagery data. *J. Geophys. Res.,* **98,** 18 501–18 514.

Liou, K. N., 1974: On the radiative properties of cirrus in the window region and their influence on remote sensing of the atmosphere. *J. Atmos. Sci.,* **31,** 522–532.

——, 1986: Influence of cirrus clouds on weather and climate processes: A global perspective. *Mon. Wea. Rev.,* **114,** 1167–1199.

——, S. C. Ou, Y. Takano, F. P. J. Valero, and T. P. Ackerman, 1990: Remote sounding of the tropical cirrus cloud temperatures and optical depth using 6.5 and 10.5 μm radiometers during STEP. *J. Appl. Meteor.,* **29,** 716–726.

Minnis, P., K. N. Liou, and Y. Takano, 1993a: Inference of cirrus cloud properties using satellite-observed visible and infrared radiances. Part I: Parameterization of radiance fields. *J. Atmos. Sci.,* **50,** 1279–1304.

——, P. W. Heck, and D. F. Young, 1993b: Inference of cirrus cloud properties using satellite-observed visible and infrared radiances. Part II: Verification of theoretical cirrus radiative properties. *J. Atmos. Sci.,* **50,** 1305–1322.

Ou, S. C., K. N. Liou, W. M. Gooch, and Y. Takano, 1993: Remote sensing of cirrus cloud parameters using advances very high resolution radiometer 3.7 and 10.9 μm channels. *Appl. Opt.,* **32,** 2171–2180.

——, ——, Y. Takano, N. X. Rao, A. J. Heymsfield, L. M. Miloshevich, B. Baum, and S. A. Kinne, 1995: Remote sounding of cirrus cloud optical depths and ice crystal sizes from AVHRR data: Verification using FIRE II IFO measurements. *J. Atmos. Sci.,* **52,** 4143–4158.

Parol, F., J. C. Buriez, G. Brogniez, and Y. Fouquart, 1991: Information content of AVHRR channels 4 and 5 with respect to the effective radius of cirrus cloud particles. *J. Appl. Meteor.,* **30,** 973–984.

Prata, A. J., and I. J. Barton, 1993: A multichannel, multiangle method for the determination of infrared optical depth of semitransparent high cloud from an orbiting satellite. Part I: Formulation and simulation. *J. Appl. Meteor.,* **32,** 1623–1637.

Russell, J. E., 1996: The retrieval of temperature and infrared optical depth of cirrus cloud using the ATSR. Ph.D. thesis, Imperial College, University of London, 219 pp. [Available from Imperial College, London SW7 2BZ, United Kingdom.]

——, R. J. Bantges, J. D. Haigh, W. L. Smith, and H. E. Revercomb, 1997: Retrieval of cirrus cloud properties from high spectral resolution IR measurements. *Proc. SPIE* (EUROPTO Series), **3220,** 60–71.

Smith, W. L., P. F. Hein, and S. K. Cox, 1990: The 27–28 October 1986 FIRE IFO Cirrus case study: In situ observations of radiation and dynamic properties of a cirrus cloud layer. *Mon. Wea. Rev.,* **118,** 2389–2401.

Szejwach, G., 1982: Determination of semi-transparent cirrus cloud temperature from infrared radiances: Application to METEOSAT. *J. Appl. Meteor.,* **21,** 384–393.

Takano, Y., and K. N. Liou, 1989: Solar radiative transfer in cirrus clouds. Part I: Single-scattering and optical properties of oriented hexagonal ice crystals. *J. Atmos. Sci.,* **46,** 3–19.

Vass, P., and M. Handoll, 1991: UK ERS-1 reference manual. DCMA-EOS-ED-0001, 189 pp. [Available from EODC Documentation and Information Service, Earth Observation Data Centre, Space Department, Royal Aerospace Establishment, Farnborough, GU14 6TD, United Kingdom.]

Wu, M. L., 1987: A method for remote sensing the emissivity, fractional cloud cover and cloud top temperature of high-level, thin clouds. *J. Climate Appl. Meteor.,* **26,** 225–233.